Mobility relaxation and electron trapping in a donor/acceptor copolymer

Marcel Schubert,[1] Eduard Preis,[2] James C. Blakesley,[1] Patrick Pingel,[1] Ullrich Scherf,[2] and Dieter Neher[1]
[1]*University of Potsdam, Institute of Physics and Astronomy, Karl-Liebknecht-Str. 24-25, 14476 Potsdam, Germany*
[2]*Bergische University Wuppertal, Macromolecular Chemistry, 42119 Wuppertal, Germany*
(Received 6 September 2012; published 17 January 2013)

To address the nature of charge transport and the origin of severe (intrinsic) trapping in electron-transporting polymers, transient and steady-state charge transport measurements have been conducted on the prototype donor/acceptor copolymer poly[2,7-(9,9-dialkyl-fluorene)-alt-5,5-(4′,7′-di-2-thienyl-2′,1′,3′-benzothiadiazole)] (PFTBTT). A charge-generation layer technique is used to selectively address transport of the desired charge carrier type, to perform time-of-flight measurements on samples with <200 nm thickness, and to combine the time-of-flight and the photocharge extraction by linearly increasing voltage (photo-CELIV) techniques to investigate charge carrier dynamics over a wide time range. Significant trapping of free electrons is observed in the bulk of dioctyl-substituted PFTBTT (alt-PF8TBTT), introducing a strong relaxation of the charge carrier mobility with time. We used Monte-Carlo simulation to simulate the measured transient data and found that all measurements can be modeled with a single parameter set, with the charge transport behavior determined by multiple trapping and detrapping of electrons in an exponential trap distribution. The influence of the concomitant mobility relaxation on the transient photocurrent characteristics in photo-CELIV experiments is discussed and shown to explain subtle features that were seen in former publications but were not yet assigned to electron trapping. Comparable studies on PFTBTT copolymers with chemical modifications of the side chains and backbone suggest that the observed electron trapping is not caused by a distinct chemical species but rather is related to interchain interactions.

DOI: 10.1103/PhysRevB.87.024203 PACS number(s): 73.50.Dn, 73.61.Ph, 72.20.Fr, 72.40.+w

I. INTRODUCTION

The effectiveness of conjugated polymers in applications, not only in organic photovoltaic cells, light-emitting diodes (LEDs), and organic field-effect transistors (OFETs) but also in more complex, integrated smart systems, depends on their ability to transport charge. Thus, from the first days of organic electronics, the investigation and description of charge transport phenomena provided the basis of a deeper understanding and further optimization of conjugated materials. In that sense, the charge carrier mobility is mostly used to describe the charge transport capability of an organic semiconductor. Unfortunately, the mobility represents one of the most complex parameters, as it is influenced by temperature, electric field, and charge carrier density. These dependencies are further related to the shape and width of the density of states (DOS) distribution. Numerous investigations and models have attempted to describe and understand the influence of these parameters on the charge carrier mobility. Two popular semiempirical models are the Gaussian disorder model (GDM) and the multiple trapping (MT) and release model. The GDM describes charge transport by hopping of localized charges between transport sites that are Gaussian distributed in energy and space.[1] In contrast to this, the MT model treats charge carriers as free until they become trapped in an (exponential) density of trap states (DOTS).[2] Displacement of these charges requires that they be thermally excited back to the transport manifold. Both the GDM and the MT model have been extensively used to analyze steady-state current voltage characteristics of uni- and bipolar polymer-based devices,[3,4] to understand the dependence of the mobility on carrier and dopant concentration,[4–7] to quantify the energy alignment at the polymer–metal contacts,[8,9] and to model charge carrier mobilities measured by transient photocurrent techniques as a function of field and temperature.[10–13] One unique property of MT with an exponential trap distribution is that the energetic distribution of carriers generated, e.g., by pulsed illumination in a transient photocurrent experiment never adopts a stationary state but rather decays continuously in energy. Tiedje and Rose pointed out that under these particular conditions, the time dependence of mobility follows a simple power law: $\mu(t) = \mu_0 \cdot (t/t_0)^{\alpha-1}$, with $\alpha < 1$ describing the energetic width of the exponential trap distribution relative to thermal energy.[2] Interestingly, few reports demonstrate explicitly the power-law decay of the mobility over a considerable range in mobility and time. Devizis *et al.* investigated the mobility relaxation of a polyspirobifluorene derivative in the pico- to nanosecond time regime. A very high mobility was found for free charges directly after photogeneration, followed by a power-law decay over five orders in time.[14] Surprisingly, in contradiction to the GDM and the MT model, this relaxation was found to be independent of temperature,[15] which underlines the importance of further experimental investigations of these phenomena. Besides the relaxation process on ultrashort timescales, relaxation processes on the micro- to millisecond regime were mostly reported for blends consisting of an electron-donating and electron-accepting compound.[11,16,17] Here, the intermixing on molecular dimensions seems to introduce a variety of additional electronic states that significantly influences charge transport and recombination, which are both highly relevant for device operation. However, neither a proper explanation on the origin of the mobility relaxation nor a description of the current transients under such conditions has existed until now; both of these primarily motivate this article.

Here, we report temporal relaxation of the electron mobility covering the microsecond range in the well-known polymer poly[2,7-(9,9-dialkyl-fluorene)-alt-5,5-(4′,7′-di-2-thienyl-2′,1′,3′-benzothiadiazole)] (PFTBTT), also called PFDTBT or APFO-3.[18] It was one of the first donor/acceptor-type copolymers designed especially for use in bulk heterojunction organic solar cells. The relatively small optical band gap of 1.88 eV and the low-lying highest occupied molecular orbital render this polymer one of the most promising materials for organic photovoltaics. When used as a polymeric donor, in combination with soluble fullerene derivatives, power conversion efficiencies (PCEs) of $\leqslant 5\%$ have been achieved, with the exact value depending in part on the position of side-chain attachment to the PFTBTT backbone.[19–21] In combination with PCBM, Veldman *et al.* predicted that PCEs as high as 9% should be achievable.[22] Recently, a 2% all-polymer solar cell was presented by Mori *et al.* that incorporated PFTBTT as the electron-accepting material.[23] This value represents one of the best efficiencies for all-polymer solar cells. He *et al.* also reported excellent all-polymer solar cells with a more soluble derivative of PFTBTT, poly((9,9-dioctylfluorene)-2,7-diyl-alt-[4,7-bis(3-hexylthien-5-yl)-2,1,3-benzothiadiazole]-2′,2″-diyl) (F8TBT), with PCEs of 1.9%.[24] This demonstrates that PFTBTT-based copolymers can work as both the electron-donating and the electron-accepting components, meaning that these copolymers are capable of transporting electrons and holes with adequate mobilities. To the best of our knowledge, it is the only material for which the ambipolar nature of charge transport has been successfully transferred to efficient solar cells. Such polymers may gain increasing interest, since they offer the opportunity to produce ternary blends with cascade photocurrent generation.[25] This motivated studies of the charge transport properties in blend layers. Most of these studies addressed the hole mobility of the polymer in blends with soluble fullerenes.[26–28]

However, there are several reports of electron trapping in blends of F8TBT with the hole-transporting polymer poly(3-hexylthiophene) (P3HT), despite the rather good performance of these blend devices. Hwang *et al.*, numerically modeled the transient photocurrent response of a F8TBT:P3HT blend by assuming a MT mechanism for the electron transport.[29] It was found that the free electron mobility of $\mu_e = 1 \times 10^{-3}$ $cm^2V^{-1}s^{-1}$ is reduced by more than two orders of magnitude on timescales relevant for charge extraction in solar cell devices under working conditions. The trap-dominated transport in pristine F8TBT was further confirmed by the observation of highly dispersive photocurrent transients.[28] A comparison to blends with a fullerene derivative as the electron-accepting compound implied that the solar cell performance of F8TBT:P3HT blends is limited by the proposed trapping process.[30]

In the following, we present a detailed analysis of the charge transport in PFTBTT-based copolymers. We first show the ambipolar nature of charge transport in the alternating copolymer poly[2,7-(9,9-dioctylfluorene)-alt-5,5-(4′,7′-di-2-thienyl-2′,1′,3′-benzothiadiazole)] (alt-PF8TBTT). After that, transient electron transport is addressed with the photocharge extraction by linearly increasing voltage (photo-CELIV) technique. To investigate electron transport and trapping, a thin charge-generation layer (CGL) is introduced that enables time-of-flight (TOF) and time-delayed time-of-flight (td-TOF) measurements on sub-200-nm-thick films. Monte-Carlo (MC) simulations based on the MT formalism are performed to rationalize the experimental current transients. Finally, side chain- and backbone-modified PFTBTT copolymers are investigated to elucidate the origin of the electron trapping in alt-PF8TBTT.

II. DEVICE PREPARATION AND EXPERIMENTAL TECHNIQUES

A. Polymer synthesis

The monomers 2,7-dibromo-9,9-dialkyl fluorene[31–33] and dibromo/distannylated TBTT[32,34–36] have been synthesized according to literature procedures. Two batches of alt-PF8TBTT with a molecular weight M_n of 5000 g/mol and polydispersity indices (PDIs) of 2.5 and 2.0 were synthesized in a Stille-type cross-coupling reaction using distannylated TBTT and 2,7-dibromo-9,9-dialkylfluorenes with $Pd(PPh)_2Cl_2$.[34,35] No differences in the charge transport properties were observed between the batches. Films were prepared by dissolving PFTBTT in chloroform and spin coating the solution at a speed of 1500 rpm. The standardized preparation conditions include thermal annealing of the films for 10 min at 140 °C. The alternating copolymer poly[2,7-(9,9-dioctyldodecylfluorene)-alt-5,5-(4′,7′-di-2-thienyl-2′,1′,3′-benzothiadiazole)] (alt-PF8/12TBTT) with elongated alkyl chains was synthesized in a similar way as alt-PF8TBTT; it had a M_n of 8000 g/mol, while the PDI was 2.1.

Poly[2,7-(9,9-dioctylfluorene)-co-5,5-(4′,7′-di-2-thienyl-2′,1′,3′-benzothiadiazole)] (part-PF8TBTT) is a "partially" alternating PFTBTT copolymer prepared in a Stille-type cross-coupling reaction of the three monomers distannylated TBTT, dibromo TBTT, and 2,7-dibromo-9,9-dioctylfluorene. The feed ratio of these three monomers was 50:10:40, respectively. The resulting copolymer possesses a molecular weight of 4500 g/mol and a PDI of 1.5. The chemical structures of the described copolymers are summarized in Fig. 1.

B. Device preparation

OFETs were built on highly doped silicon substrates on which a silicon oxide (SiO_2) layer of ∼300 nm served as the gate dielectric. The SiO_2 surface was further treated with hexamethyldisilazane to remove electron traps that naturally exist on top of bare SiO_2.[37] The width and length of the channel and the areal capacitance of the device are 14.85 cm, 100 μm, and 11.9 nF/cm^2, respectively. Gold source and drain electrodes were thermally evaporated at a pressure of $\sim 10^{-6}$ mbar.

Devices for photo-CELIV, TOF, and td-TOF measurements were built on prestructured indium tin oxide-coated glass substrates on which a 50-nm-thick layer of PEDOT:PSS (Clevios P VP AI 4083) was spin coated in air and dried at 180 °C for 10 min inside of a nitrogen-filled glove box. In case P3HT was used as CGL, it was spin coated on top of PEDOT:PSS and thermally annealed at 180 °C for 10 min.

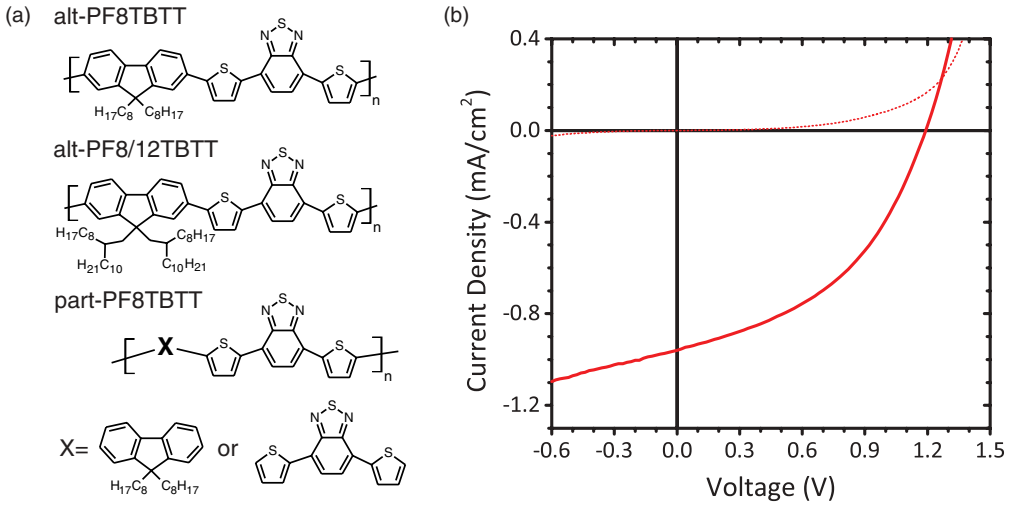

FIG. 1. (Color online) (a) Chemical structures of the PFTBTT copolymers. (b) Solar cell device characteristic of 40-nm alt-PF8TBTT on top of a P3HT CGL under AM 1.5G illumination at 100 mW/cm^2 (straight red line) and in the dark (dotted red line).

Washing this layer three times with chlorobenzene resulted in the formation of a 3-nm P3HT interlayer (as proven by optical absorption measurements).[38,39] The PFTBTT copolymers were spin coated from a chloroform solution, and the devices were completed by evaporation of 20-nm samarium covered by 100-nm aluminum. The active area of the final devices is 1 mm^2. To protect the samples against oxidization in air, a thin glass substrate fixed with a two-component epoxy resin was used for encapsulation.

C. Transient photocurrent experiments

Optical excitation for TOF and pulsed extraction techniques came from an optical parametric oscillator fed by the third harmonic of a neodymium-doped yttrium aluminum garnet laser working at 500 Hz (Ekspla, NT series). The excitation wavelength was 600 nm, and the pulse width was 6 ns. Samples were mounted in a homemade sample holder or in a closed-cycle He cryostat. Currents were amplified by a Femto DLH current amplifier and recorded by a Yakagawa 500-MHz storage Oscilloscope. For all transient measurement techniques, the intensity of the laser was adjusted to keep the photogenerated charge $<10\%$ of the capacitive charge to ensure that neither the internal field redistributes due to the photogenerated charge nor the transients were influenced by bimolecular recombination.[40] The corresponding charge carrier densities were $<5 \times 10^{21}$ m^{-3} in all cases. This ensured that all experiments were performed in the low charge carrier density regime, where the bulk mobility is not affected by the charge carrier density.[5,7] For td-TOF measurements, our sample design allowed a voltage pulse rise time of <20 ns. In all transient measurements, the internal electric field was corrected by the built-in voltage. A value of 1.2 eV was found, determined as the voltage at which no photocurrent flows immediately after excitation.

D. MC simulation

In general, the simulation of current transients with hopping models needs to consider all possible jumps between all states within the DOS. However, in the low-energy tail of the DOS, the distance between sites of approximately the same energy is large. Thus, for charges in tail states to move, thermal excitation to sites close to the center of the DOS, with larger electronic coupling, is necessary.

Charge transport occurs predominately in a small energy range around a "transport energy." The MT model simplifies this situation by defining a "mobility edge," which is equivalent to the transport energy, and divides the DOS into free states and trap states. Carriers occupying states above the mobility edge are assumed to be free and have a fixed, constant mobility μ_0, while carriers occupying states below the mobility edge (DOTS) are trapped and have zero mobility. We assumed an exponential DOTS, which was motivated by the observed power-law decay of the photocurrent in the TOF experiments (described later). The simplicity of the MT model allows fast MC simulations[41] of current transients in seconds on a desktop computer, as opposed to the cluster-scale computation resources required for performing MC simulations with more complex hopping models.

Our MC simulation considers the motion of individual, noninteracting charge carriers. At the beginning of the simulation, each carrier is treated as free at a displacement $x = 0$. The time until the first trapping event is randomly sampled from an exponential distribution with mean time t_{trap}. During this interval, the carrier moves at a velocity $F\mu_0$, where F is the electric field, and generates a corresponding displacement current $eF\mu_0/d$ in the external circuit, where d is the film thickness and e is the elementary charge. At the end of this interval, the carrier becomes trapped. The energy of the trap site E is sampled at random from the exponential DOTS with mean trap energy of E_0. The carrier then remains immobile, generating no displacement current, until it becomes detrapped. The dwell time the carrier remains in the trapped state is randomly sampled from an exponential distribution with mean time $t_{\text{trap}} \exp(E/k_{\text{B}}T)/N_{\text{eff}}$, determined by detailed balance, where $k_{\text{B}}T$ is the thermal energy and $N_{\text{eff}} = N_{\text{trap}}/N_{\text{free}}$ is the effective concentration of trap states, the ratio between the densities of trap and those of free states.

The trapping and detrapping process is repeated until the charge carrier reaches the counter electrode $x = d$. Current transients were constructed by averaging 10^5 carriers to give noise-free curves.

An effective mobility μ_{eff} of a charge carrier at any time is given by the free carrier mobility multiplied by the fraction of carriers in a free state. When simulating transient photocurrents with a long delay between excitation and extraction, it was necessary to include a field-dependent detrapping rate to accurately fit the measured transients. This was implemented by increasing the detrapping rate by a factor of $\exp(aF/k_{\text{B}}T)$ (up to $aF = E$). The fitting parameter a loosely represents the typical hopping distance from a trap state to a nearby free carrier state in the downfield direction.[42]

III. RESULTS AND DISCUSSION

A. Electron transport in alternating PF8TBTT

Two contradicting views of the charge transport properties of PFTBTT-based OFETs can be found in literature. While work by Muller *et al.*[26] and Andersson *et al.*[43] did not reveal electron transport in pristine PFTBTT OFETs, McNeill *et al.* nicely demonstrated ambipolar behavior of F8TBT in a light-emitting OFET.[44] We performed OFET measurements in bottom gate–top electrode geometry with a silanized SiO_2 gate insulator (displayed in Fig. S1 of the supplementary material),[71] which clearly showed ambipolar charge transport in alt-PF8TBTT and reveal mobilities for holes and electrons of $\mu_{\text{h}} = 2 \times 10^{-3}$ $\text{cm}^2\text{V}^{-1}\text{s}^{-1}$ and $\mu_{\text{e}} = 4 \times 10^{-4}$ $\text{cm}^2\text{V}^{-1}\text{s}^{-1}$, respectively, that are comparable to those reported in Ref. 44. Therefore, we conclude here that alt-PF8TBTT can be regarded as an ambipolar material with overall good electron transport, consistent with the observation of the excellent acceptor properties of alt-PF8/12TBTT in organic solar cells, where sufficiently high electron mobility is a prerequisite.[23]

In order to address bulk transport properties of alt-PF8TBTT, we applied different transient photocurrent techniques. A common technique for determining charge carrier mobilities is the photo-CELIV technique.[45] Here, photogenerated charges are continuously accelerated by a linear increasing voltage. Given a homogeneous charge carrier density, extraction of charge carriers at one side of the device sets in simultaneously, leading to a characteristic maximum in the current signal from which the electron mobility can be calculated. In addition, the delay time between the pulsed excitation and the beginning of the extraction pulse t_{del} can be varied, which allows the investigation of charge recombination or charge relaxation phenomena. The advantage of CELIV is that it can be applied to thin organic layers of some 100 nm. Thus, charge transport can be studied on spatial and temporal dimensions that are relevant for active devices like solar cells or LEDs.

Photo-CELIV transients of a 205-nm-thick film of alt-PF8TBTT are displayed in Fig. 2(a). Transients are shown for several delay times, spanning three orders of magnitude in time from 150 ns to 100 μs. A distinct extraction peak is seen in the photo-CELIV transients for a short delay, while with increasing t_{del}, the maximum current decreases and the time t_{max}, which is the time between the beginning of the extraction

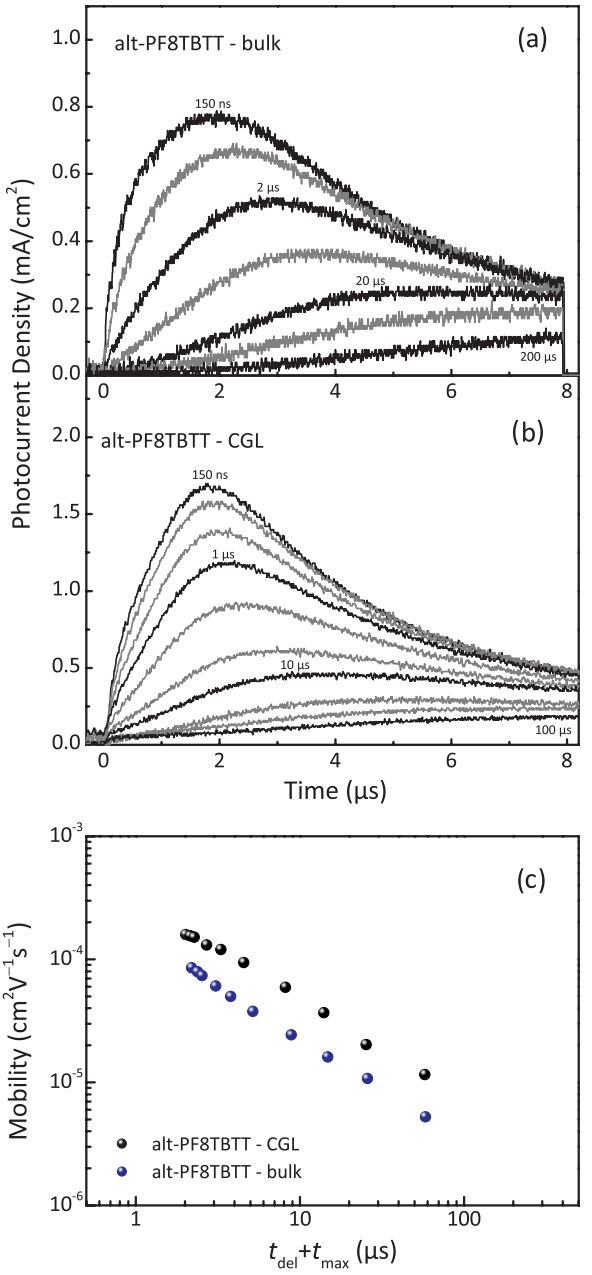

FIG. 2. (Color online) Room-temperature photo-CELIV transients at various delay times for (a) a 205-nm-thick single layer of alt-PF8TBTT and (b) a 170-nm alt-PF8TBTT layer with an additional 3-nm P3HT CGL. The capacitive loading current j_{cap} was subtracted to visualize photocurrents only. Transients are shifted to $t = 0$, which denotes the beginning of the extraction ramp that had slopes of 0.86 V/μs (bulk) and 1.09 V/μs (CGL). To avoid charge extraction during the delay time, a forward bias of 1.2 V was applied during photoexcitation and delay. (c) CELIV mobilities μ_{CELIV} deduced from experiments on bulk and CGL devices, plotted over $t_{\text{del}} + t_{\text{max}}$ (for calculation, see text).

pulse and the time at the photocurrent maximum, increases. In addition, all transients exhibit a rather pronounced tail, whose height is only slightly affected by the delay time. For delay times above 20 μs, the transients have no distinct maximum and instead consist of a slowly increasing current. Such characteristic features were also observed by others,[11,16,17,46,47]

but their origin has not been discussed so far. In the low carrier density regime, the corresponding mobility μ_{CELIV} is obtained via $\mu_{\mathrm{CELIV}} = 2d^2[3t_{\mathrm{max}}^2 A']^{-1}$, where A' is the voltage rise speed.[48] The calculated mobility as a function of delay time is displayed in Fig. 2(c). This plot shows a continuous decrease of μ_{CELIV} with increasing delay time. This decay, as well as the unusual shape of the current transients, suggests that the mobility must be a function of time throughout the entire temporal range considered here. In this context, the initial rise of the CELIV transients is highly nonlinear for short delay times, in contrast to the predicted linear rise for a time- and field-independent mobility.[48] Note that, the nature of the mobile (faster) charge carrier type, either electron or hole, can in general distinguished in a CELIV experiment, and both carrier types can significantly contribute to the current.[49] Indeed, our OFET measurements suggest that in alt-PF8TBTT, both types of charge carriers are mobile, which therefore represents a fundamental problem whenever photogenerated carriers are generated over the entire layer thickness. Thus, the understanding of the current transient and a definitive identification of the electron transport in alt-PF8TBTT is, at this point, not possible and requires a more sophisticated measurement technique.

An elegant approach to avoid the difficulties of the standard CELIV measurement in distinguishing charge carrier types is to insert a CGL.[50] Here, a thin photoactive layer is inserted into the device structure to create a planar heterojunction (PHJ) between the CGL and the transport layer, the latter being the material under study. After excitation, excitons predominantly dissociate at the PHJ, generating free charge carriers. The polarity of the generated carriers inside the transport layer depends only on the relative position of the energy levels between generation and transport layer. As a further benefit of the CGL technique, the optical field profile within the device may not be known for the exact analysis of the transients, since free charge generation is almost exclusively at the PHJ.[50] Here, we apply this technique to measure carrier mobilities in thin polymer layers <200 nm using photo-CELIV and TOF, where for the latter technique, several-micrometer-thick layers are normally required.

To study electron transport in PFTBTT copolymers, we introduced a P3HT CGL between the PEDOT:PSS anode and the PFTBTT transport layer. In this combination, the CGL acts as a donor while PFTBTT represents the electron-accepting and electron-transporting phase.[23,44,51] A typical current–voltage characteristic of a solar cell device comprising a 3-nm P3HT CGL and a 40-nm- thin alt-PF8TBTT layer is displayed in Fig. 1(b). This cell gives a reasonable PCE of 0.5% under 100 mW/cm^2 air mass 1.5 global (AM 1.5G) illumination with a short circuit current density of $\sim$1 mA/cm^2. In addition, the external quantum efficiency at the excitation wavelength of 600 nm of this device is $\sim$100 times higher than of a device without CGL. This demonstrates that the photocurrent originates from free carriers generated at the PHJ.

Photo-CELIV current transients of devices comprising a P3HT CGL recorded over the range of delay times, as for the bulk device, are displayed in Fig. 2(b). The general characteristics of the photocurrent are comparable for the CGL and the bulk device, including the strong shift of t_{max} with increasing t_{del}, the pronounced tail at the end of the extraction pulse, and the slowly increasing current at high delay times. This result strongly implies that electrons also determine the transient current in the bulk photo-CELIV experiment. The corresponding electron mobility values were extracted from the maximum of the photo-CELIV transient t_{max} in the CGL device. Assuming that charges are generated only at the interface to the thin CGL and accelerated by a linear increasing field $E(t) = A't/d$ with a slope of A', the mobility is simply derived from $s(t) = \int v(\tau)d\tau = \mu \int E(\tau)d\tau$. Assuming that $s(t_{\mathrm{max}}) = d$ yields

$$\mu_{\mathrm{CELIV,CGL}} = \frac{2d^2}{t_{\mathrm{max}}^2 A'}. \tag{1}$$

This formula is correct in that the CGL is much thinner than the layer thickness d and that the photogenerated charge is much smaller than the capacitive charge stored at the electrodes $Q_{\mathrm{photo}} \ll Q_{\mathrm{cap}}$ (see also Fig. S2 of the supplementary material).[71] The latter condition rules out that space charges distort or screen the external applied field. Equation (1) differs by a factor of 1/3 from the case of an initially homogeneously distributed charge density. Mobilities obtained by Eq. (1) are displayed in Fig. 2(c). Again, the mobility drops continuously over a time span of two orders of magnitude, following a power-law decay with an exponent of $\sim 0.81 \pm 0.01$. To summarize, the photo-CELIV transients in bulk and CGL devices both reflect the electron transport characteristics of alt-PF8TBTT and reveal a pronounced mobility relaxation over two orders in time.

One drawback of photo-CELIV is that extraction is with a nonconstant, linearly rising electric field. Therefore, care must be taken when interpreting CELIV transients, where the photocurrent maximum appears at different times and consequently at different electric fields. To circumvent this problem, we performed experiments using the td-TOF method. Here, a rectangular voltage pulse is applied to the sample after an adjustable delay time. Thus, this technique merges advantages of photo-CELIV and TOF. To the best of our knowledge, this is the first time that transport dynamics have been investigated using the td-TOF technique. A detailed description of the setup and working principle can be found in a recent publication by Kniepert *et al.*[52]

Experimental td-TOF transients are displayed in Fig. 3, together with the standard TOF transient for a P3HT CGL device with a 170-nm-thick alt-PF8TBTT layer. The top electrode was positively charged to probe the transport of electrons. No transients were detected when the polarity is changed, which proves that electrons are efficiently generated at the CGL and transported through the alt-PFTBTT layer. In td-TOF, a constant voltage of 1.2 V was applied during the delay time as in the CELIV experiment to avoid carrier extraction. Then, the voltage is switched to -0.5 V (top electrode positively charged within 20 ns) to create an extraction field. The same voltage of -0.5 V was applied in the regular TOF experiment.

The regular TOF current transient displayed in Fig. 3 is strongly dispersive, and its initial decay follows a strict power-law dependence of $j(t) \propto t^{\alpha-1}$. As pointed out in Sec. I, such time dependence is characteristic for charge transport that is dominated by MT and detrapping in an exponential DOS distribution $g(E) = N_t k_B^{-1} T_0^{-1} \exp[-(E_L - E)/(E_0)]$ of

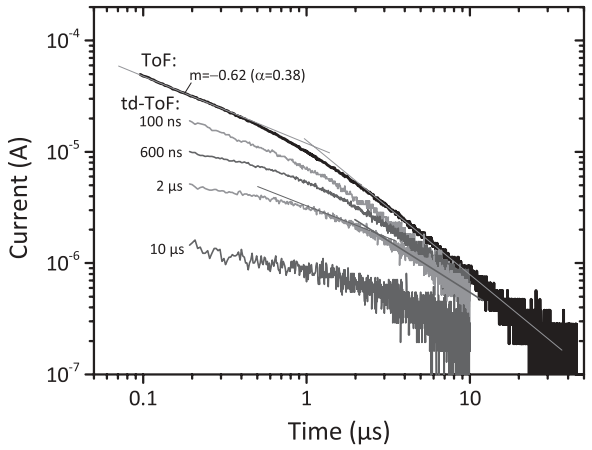

FIG. 3. TOF (black) and td-TOF (light and dark gray) current transients at a temperature of 295 K and an extraction field of 1×10^7 V/m. td-TOF transients are shown for several delay times to display the increase in the transit time. The thickness of the alt-PF8TBTT active layer was 170 nm. Straight lines are a visual guide for the two linear regions.

trapping states, where N_t is the total DOTS, $E_0 = k_B T_0$ is the characteristic energy, E_L is the energy of the lowest unoccupied molecular orbital, k_B is Boltzmann's constant, and T_0 is the characteristic temperature.[13] The slope parameter α is then given by $\alpha = T/T_0$. For the data shown in Fig. 3, the double-logarithmic slope $m = \alpha - 1 = -(1 - k_B T/E_0)$ is equal to -0.62, which yields E_0 67 meV for alt-PF8TBTT, corresponding to a characteristic temperature of 775 K. In this model, the current at a given time is directly proportional to the effective mobility in the organic semiconductor. In other words, the power-law decay of the current reflects the time dependence of the mobility. Above 1 μs, the TOF transient's slope changes, indicative of the arrival of the fastest electrons at the counter electrode. At an internal field of 1×10^7 V/m, the transit time of the electrons is $\sim$1 μs. From this, the electron mobility was calculated to be 1.7×10^{-4} cm^2/Vs, close to the mobility obtained by photo-CELIV measurements at very short delay times [Fig. 2(c)]. This value for the electron mobility is even higher than reported bulk hole mobilities in pure PFTBTT,[27] showing that in the bulk, electrons might be the faster type of charge carriers. The small thickness of 3 nm and the high hole mobility in regioregular P3HT of $\sim 1 \times 10^{-4}$ cm^2/Vs[53] sets the transit time of holes in the CGL to $\sim$1 ns, orders of magnitude faster than the observed transit time, again confirming that we are able to probe exclusively the electron transport through the alt-PF8TBTT layer.

For short delay times, td-TOF and TOF show comparable current transients with similar transit times. With increasing delay time, the initial slope of the td-TOF transient decreases and reaches a nearly constant value at a delay time of 10 μs. Also, the change in slope is seen at later times, suggesting a larger transit time. This is exemplarily shown in Fig. 3 for the td-TOF transient after a 2-μs delay. The calculated mobility is 7×10^{-5} cm^2/Vs, which is comparable to the value obtained by photo-CELIV at the same delay. Thus, our td-TOF measurements unambiguously reveal a pronounced time dependence of the mobility.

B. Simulation of current transients

The qualitative agreement between the results from td-TOF (constant field) and those from photo-CELIV (linearly increasing field) measurements as described previously suggests that time-dependent electron mobility in an exponential DOTS rather than its explicit field dependence governs the CELIV transients at different delay times. To confirm this, a numerical MC simulation based on a MT model was used to simulate the measured current transients. The algorithm of the simulation is described is Sec. II D, and best fits are displayed in Fig. 4. The parameters used for these simulations are summarized in Table I and were determined as follows. First, the initial current decay m of the TOF transient in Fig. 3 is used to fix the trap energy E_0 to 67 meV. In a next step, the free carrier mobility μ_0, the trap time t_{trap}, and the effective trap density N_{eff} were chosen to accurately reproduce photo-CELIV transients at very short delay times. Then t_{trap} and N_{eff} were fixed. Finally, the parameter a describing the field-assisted detrapping is

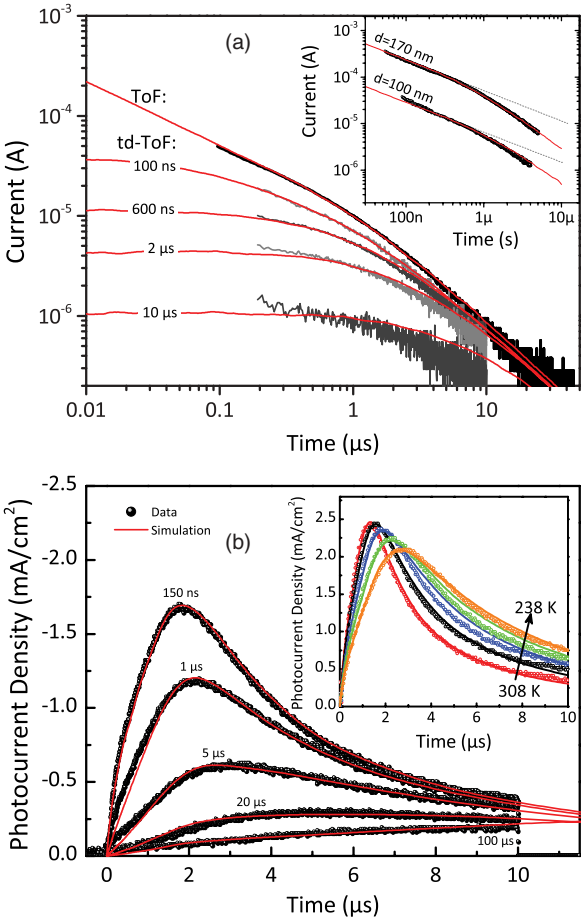

FIG. 4. (Color online) Comparison of MC simulation results with measured transients obtained by (a) TOF and td-TOF and (b) photo-CELIV. The data are taken from Figs. 2 and 3. Delay times are indicated at each transient. Inset (a): Room-temperature TOF transients of CGL devices with a 170- and a 100-nm-thick alt-PF8TBTT layer at a field of 1×10^7 and 5×10^6 V/m, respectively. The dotted lines represent the extension of the initial current decay with a slope of $m = -0.62$. Inset (b): Photo-CELIV transients after a 150-ns delay at 308, 287, 269, 256, and 238 K.

TABLE I. Fit parameters used for the simulation in Fig. 4.

Parameter	Description	Value
t_{trap}	Trap time	0.5 ns
E_0	Trap energy	67 meV
N_{eff}	DOTS/density of free states	0.05
μ_0	Free carrier mobility	$2.3{\cdot}10^{-3}$ $cm^2V^{-1}s^{-1}$ (TOF)
		$2.8{\cdot}10^{-3}$ $cm^2V^{-1}s^{-1}$ (CELIV)
a	Field activation length	1.1 nm
d	Active layer thickness	170 nm
F	Extraction field (TOF, td-TOF)	1×10^7 V/m
A'	Voltage ramp (photo-CELIV)	1.09 V/μs

introduced into the simulation by fitting the long delay time transients, while μ_0 was allowed to slightly vary until all photo-CELIV transients were accurately described with the same set of parameters. The mobility is treated as field independent, in good agreement with our measurements (see Fig. S3 of the supplementary material).[71] Every feature of the experimental photo-CELIV transients for different delay times and temperatures is reproduced by the simulation, including the pronounced shift of the current maximum with increasing delay, which resembles the power-law mobility decay shown in Fig. 2(c). The simulation also reproduced TOF and td-TOF data with the same set of parameters. Here, the current of a second device with an active layer thickness of only 100 nm is shown for comparison. This demonstrates that the MT model with an exponential trap distribution provides an excellent description of the data for all experimental techniques, temperatures, and delay times considered here. Regarding the physical meaning of the simulation parameters, the three parameters μ_0, t_{trap}, and N_{eff} do not define a unique set of parameters, meaning that a change of one of these parameters can be compensated by the other to give the same transient. Rather, it is the experimentally found trap energy E_0 that critically determines the width and tail of the photo-CELIV transients. Thus, E_0 determines not only the slope of the photocurrent decay in TOF measurements but also the primary shape of the photo-CELIV transients, which unequivocally connects the different experimental techniques investigated here by this single parameter.

The good agreement between the measured and the simulated data allows us to explore general aspects of the influence of charge carrier trapping on transient photocurrent experiments. A dominant feature of the td-TOF transients is the reduced initial slope of the current with increasing delay time, which is quite well reproduced by the simulation. The reason for this is that for a power-law decay, the rate at which mobility changes with time becomes smaller for increasing delay. Therefore, the mobility in a sample measured after prolonged delay is nearly constant on the timescale of carrier extraction, and so is the initial photocurrent in a log–log presentation. The same phenomenon should affect photo-CELIV measurements, where we observe a rather linear increase of the initial photocurrent with extraction time after long delay, indicative of a constant mobility.

Surprisingly, although the shape of the photo-CELIV transients is reproduced with great accuracy by the simulation, mobilities extracted from the photo-CELIV (and td-TOF) transients for different delays are about one order of magnitude larger than the effective mobility μ_{eff} of the charge carriers at time $t_{del} + t_{max}$. In accordance to the MT model, μ_{eff} is defined as the product of the fraction of free charge carriers times the free carrier mobility $\mu_{eff} = \mu_0 \cdot \phi$ and is obtained directly from the simulation by calculating the fraction of the mobile (free) charge concentration to the overall charge concentration, $\phi = N_{free}/(N_{free} + N_{trap})$ (black solid line in Fig. 5). Furthermore, the mobility decay in the simulation (and in the initial TOF transients) perfectly matches a power-law decay with an exponent of $m = -0.62$, while the mobility decay derived from the maximum of the photo-CELIV transients with increasing delay time is much faster (slope of $m = -0.81$, Fig. 5). We might propose that the overall larger mobility derived from the photo-CELIV experiment is due Eq. (1) assuming a constant mean carrier mobility. However, for a power-law decay, the carrier mobility might be substantially higher at the beginning of the voltage ramp than at t_{max}. To address this issue, we derived an expression for t_{max} in considering the mobility relaxation due by a MT process. For this, the time-dependent effective mobility has been parameterized by

$$\mu(t + t_{del}) = \mu_0 \cdot ((t + t_{del})/t_{trap})^{\alpha-1}. \quad (2)$$

Using the parameters from Table I, Eq. (2) perfectly resembles the effective mobility obtained from the MC simulation. The average path length s of a carrier drifting in a time-dependent electric field $E(t)$ with a time-dependent mean mobility is $s(t) = \int_0^t \mu(t' + t_{del}) \cdot E(t')dt'$. Here, extraction commences

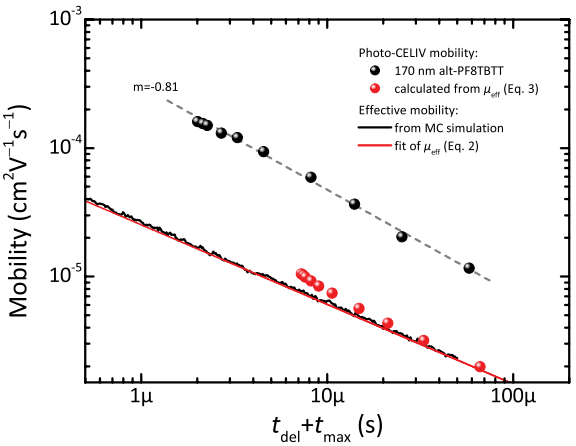

FIG. 5. (Color online) Comparison of the measured and simulated mobility relaxation. Black spheres display mobilities from measured photo-CELIV transients. The effective mobility obtained from the MC simulation is shown as a black solid line, while the solid red line displays the best fit of the time-dependent mobility to a power-law relaxation according to Eq. (2). Red spheres are the correspondent apparent photo-CELIV mobilities $\mu_{CELIV,app}$, which are obtained by applying Eq. (1) to the transit time according to Eq. (3). The dashed gray line visualizes the power-law decay of the measured mobility, where the exponent was found to be $m = -0.81$. For clarity, the simulation was performed without assuming field-activated detrapping, which is shown in Fig. 6.

at $t = 0$. This equation also contains the delay time to take into account the mobility relaxation during the delay. Assuming again, that $t = t_{tr} \cong t_{\max}$ and $s(t_{tr}) = d$ gives the following equation for $t_{\max}$:

$$\frac{d^2 \cdot t_{\text{trap}}^{\alpha-1} \cdot N_{\text{eff}}^{\alpha}}{A' \cdot \mu_0} \frac{\alpha}{1-\alpha} = (t_{\max} + t_{\text{del}})^{\alpha} t_{\max} - \frac{1}{1+\alpha} \times [(t_{\max} + t_{\text{del}})^{1+\alpha} - (t_{\text{del}})^{1+\alpha}], \quad (3)$$

which can be solved numerically for delay time. Knowing $t_{\max}$, an apparent photo-CELIV mobility $\mu_{\text{CELIV,app}}$ can be calculated from Eq. (1). This is the mobility that would be extracted by the classical photo-CELIV analysis from a photocurrent transient that is subject to mobility relaxation. Values of $\mu_{\text{CELIV,app}}$ for different delay times calculated with the simulation parameters in Table I are shown by red spheres in Fig. 5. As expected, the apparent mobility resembles the underlying time-dependent effective mobility for larger delay times, but it is slightly larger than the effective mobility, where the delay time is smaller than the transit time. This is because $\mu_{\text{CELIV,app}}$ obtained from $t_{\max}$ displays a field-averaged value over the whole extraction time. Only for delay times smaller than the transit time does a significant relaxation of the mobility take place during extraction, while for delay times higher than the transit time, the mobility is rather constant at the timescale of extraction. Even for the shortest delay time considered here (150 ns), the apparent photo-CELIV mobility is only slightly larger than the effective mobility. Therefore, we can rule out that the large difference between the mobility values extracted from our experimental photo-CELIV transients using Eq. (1) and μ_{eff} is solely caused by the power-law decrease of the mean carrier mobility.

However, the calculation according to Eqs. (1)–(3) assumes that all charge carriers have the same (mean) mobility, the same relaxation rate, and with that, the same transit time. This is far from reality for a system, where random trapping and detrapping create a wide distribution of transit times. In Fig. 6, we replotted the photo-CELIV and simulated transients from Fig. 4 on a logarithmic timescale, together with the simulated time-dependent fraction of charges that have not yet reached the extracting electrode. Clearly, the current maximum in the photo-CELIV transient at short delays appears at the moment the first charge carriers (and not the majority of carriers) leave the device. For example, at a delay of 1 μs, only 3% of the initially photoinduced charge have left the device at $t_{\max}$, and most remaining carriers are trapped ($\phi = 0.007$). In other words, the position of the current maximum after a short delay is determined by the fastest charge carriers, which have undergone only a few trapping events. Consequently, photo-CELIV and TOF strongly overestimate the effective charge carrier mobility in presence of MT.

The situation is quite different for longer delay times. Here, field-induced detrapping becomes a relevant process. The introduction of a field activation process is found to be essentially important to reproduce the current tail at the end of the extraction pulse (see also simulation results without field-induced detrapping in Fig. S4 of the supplementary material).[71] Analyzing the effective mobility in Fig. 6 shows that from a certain time on, the effective mobility starts to increase. We attribute this to the steadily increasing extraction

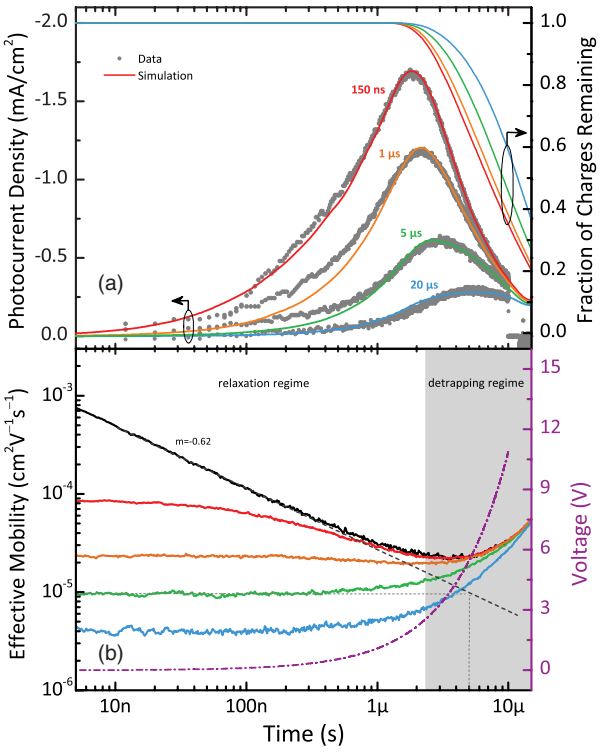

FIG. 6. (Color online) (a) Photo-CELIV (gray circles) and simulated transients (solid lines) (both left axis) together with the fraction of charges that remain in the device at time t (right axis). The abscissa is on a logarithmic scale, and $t = 0$ denotes the beginning of the extraction pulse. Colors refer to the different delay times of 0 ns (black), 150 ns (red), 1 μs (orange), 5 μs (green), and 20 μs (blue). (b) Effective mobility obtained from MC simulations for different delay times (left axis). For the effective mobility with a 0-ns delay, the fit to the linear regime in the log–log representation (dashed gray line) is also shown. It reflects the power-law mobility decay without field-activated detrapping, occurring during the delay (see also Fig. 5). This is exemplarily shown for the green curve. Here, the mobility at the beginning of the transient (starting after a 5-μs delay) is the same as for the dashed gray line at $t = 5$ μs. The time interval at which the field-activated detrapping starts to significantly increase the effective mobility is denoted as the detrapping regime. The prior time interval, where mobilities are influenced by the internal relaxation only, is denoted as the relaxation regime. The applied voltage (violet dashed–dotted line), increasing with a slope of 1.09 V/μs, is given at the right axis.

field, also displayed in Fig. 6, which increases the fraction of free charge carriers due to field-assisted detrapping. The increased mobility toward the end of the extraction pulse shifts the current maximum to later times, thus increasing $t_{\max}$. The concomitant decrease in mobility finally explains the faster power-law decay of the photo-CELIV mobility ($m = -0.81$) compared to the decay of the effective mobility ($m = -0.62$). In view of these results, TOF rather than photo-CELIV should be preferred for evaluation of characteristic trapping parameters from the current or mobility decay.

As alternatives to transient measurements, steady-state techniques are also capable of determining E_0. Figure S5 of the supplementary material[71] shows that space charge-limited

currents of alt-PF8TBTT electron-only devices[54] can be well described with a model developed by Mark and Helfrich,[55] with an exponential trap state distribution that is comparable to the one deduced from the simulation of the current transients. This further demonstrates that the processes that determine charge transport in the presence of electronic trap states are independent of the origin of the charge carriers, either injected or photogenerated, and can be consistently described within the framework of MT and release.

C. Origin of the electron traps

After having demonstrated the pronounced influence of trapping on the electron transport in alt-PF8TBTT, finding the origin of these trap states is of great interest. Because chemical impurities, e.g., residual catalyst or imperfect endcapping of polymer chains, can likely influence the charge transport of alt-PF8TBTT, we carefully revisited the synthetic procedures. For this purpose, two independent polymer batches were synthesized, from which one was further purified.[56] In addition, a third batch was provided by a collaborating laboratory. However, all three batches showed the same transport characteristics, as described in the previous section. We therefore rule out chemical impurities. This raises the question of whether trap formation is related to the specific molecular structure of the copolymer. Therefore, two different polymers with either the same polymer backbone but different side chains or the same side chain but a modified polymer backbone were synthesized. The former of these two polymers, alt-PF8/12TBTT, is a alternating PFTBTT with branched octyldodecyl side chains, while the latter, stat-PF8TBTT, contains octyl side chains and shows a partial statistical variation along the backbone (for details, see Sec. II A and Fig. 1). Here, the regular alternation of the donor and acceptor unit, as it is for alt-PF8TBTT, is disturbed by replacing a few fluorene units by TBTT segments. In Fig. 7, the photo-CELIV transients of alt-PF8/12TBTT and part-PF8TBTT CGL devices are shown for varying delay times. In contrast to the results obtained for the alt-PF8TBTT (Fig. 2), the current maximum of the two modified PFTBTT copolymers do not shift with increasing delay time. Furthermore, a distinct maximum can be observed also for high delay times of 100 μs. This means that the mobility is constant in time (at least within the observable time range from 150 ns to 100 μs). This reveals an important structure–property relationship for this type of copolymer. Emphasizing that for all polymers investigated here the synthesis, as well as the device preparation and measurement, is carried out under the same conditions, we infer that the severe mobility relaxation in alt-PF8TBTT is related to its specific molecular structure. The comparison of alt-PF8TBTT and alt-PF8/12TBTT shows that the mobility relaxation on the microsecond timescale disappears when long and branched rather than linear side chains are attached to the PFTBTT backbone. Interestingly, despite its longer side chains, alt-PF8/12TBTT exhibits significantly higher photo-CELIV mobilities than does alt-PF8TBTT. However, mobility relaxation on the timescale measured here is also suppressed when the strict alternation of the donor and acceptor unit is slightly disturbed, as seen for part-PF8TBTT. This clear correlation between the backbone structure and the specific transient transport properties rules out that the mobility relaxation observed for alt-PF8TBTT is caused to extrinsic impurities.

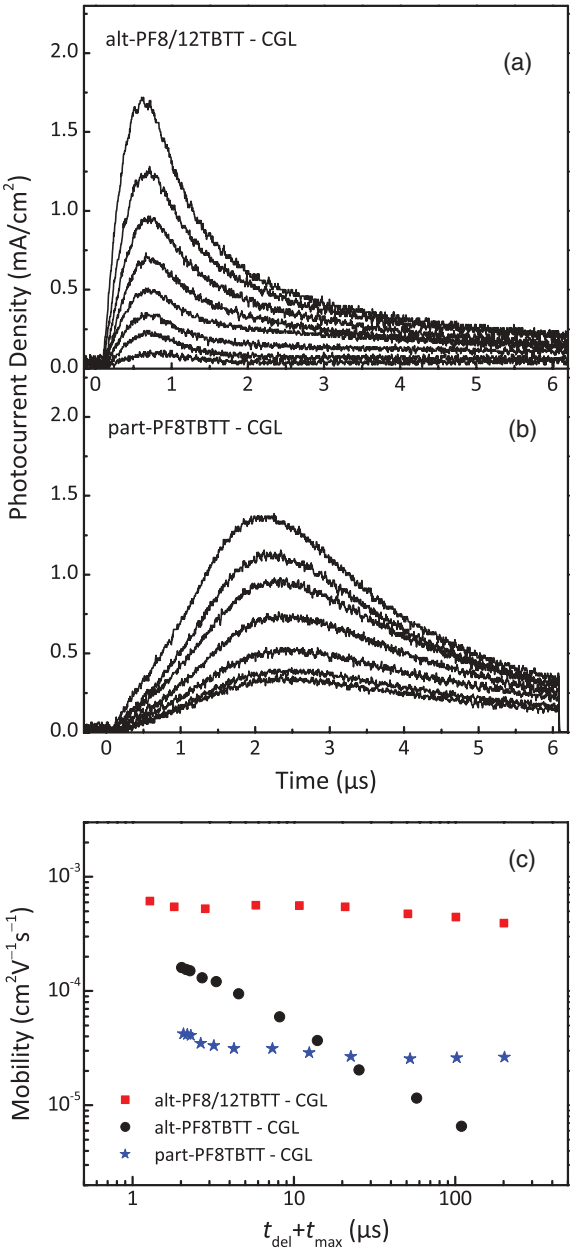

FIG. 7. (Color online) Room-temperature photo-CELIV transients at various delay times for (a) a 200-nm-thick layer of alt-PF8/12TBTT and (b) a 170-nm layer of part-PF8TBTT. In both devices, a 3-nm P3HT CGL was used. The capacitive loading current was subtracted to visualize photocurrents only. To avoid charge extraction during the delay time, a forward bias of 1.2 V was applied. (c) Mobility calculated via Eq. (1) plotted over $t_{del} + t_{max}$, together with the mobility of the alt-PF8TBTT CGL device displayed in Fig. 2.

IV. DISCUSSION

In this paper, we examine the charge transport in the donor/acceptor copolymer alt-PF8TBTT, which has been widely applied in organic solar cells. A pronounced relaxation

of the electron mobility is unambiguously proven by three transient photocurrent techniques and is the most important feature of the experiments described here. It continues over a period of at least 100 μs and is likely caused by an energetic thermalization process that follows photogeneration of free charge carriers inside the organic semiconductor.

Thermalization of photogenerated charge carriers and time-dependent mobilities has been rarely observed for conjugated polymers.[11,14–17,46,57] Österbacka *et al.* assigned the time-dependent mobility observed in regiorandom P3HT to originate from thermalization of hot, photogenerated carriers within the Gaussian DOS.[46] According to Pautmeier *et al.*, the relaxation to the thermodynamic equilibrium proceeds via a decrease in carrier mobility; however, in the case of a Gaussian DOS, it is also accompanied by a later transition to constant equilibrium mobility.[58] This so-called transition from the dispersive to nondispersive regime is predicted to shift to shorter times with increasing temperature or smaller energetic disorder, but this effect has, to best of our knowledge, not yet been observed for conjugated polymers. Recently, we showed that recombination of photogenerated charges at high carrier densities can alter photo-CELIV current transients and lead to an apparent time dependence of the CELIV mobility.[40] As the shapes of our photo-CELIV transients are independent of intensity, recombination phenomena during extraction are expected to be insignificant (see Figs. S6 and S7 of the supplementary material[71]).[59]

A model that is able to describe the continuous mobility relaxation as observed here is MT formalism, which was theoretically described by Orenstein and Kastner for an exponential DOTS.[13,60] Beside the ongoing mobility decrease, direct evidence for MT comes from the power-law decay of the TOF transients on timescales less than the transit time. To further support this, MC simulations of MT in one dimension were performed. These simulations reproduce the power-law decay of the effective mobility. Furthermore, experimental transients of several techniques and for various parameters (delay time and temperature) can be described with a single set of parameters. Thus, we are able to explain the anomalous shape of photo-CELIV transients entirely by MT, acting on the transport of a single charge carrier type only.

Our results also allow us to speculate about the origin of electron traps in the alt-PF8TBTT copolymer. Chemical defects that act as electronic trap states, i.e., hydrated oxygen complexes, were recently proposed by Nicolai *et al.* to rationalize widely observed trap-limited electron currents in many semiconducting polymers, including alt-PF10TBTT.[61] Furthermore, Kuik *et al.* demonstrated that the prominent keto defect in poly(9,9-dioctylfluorene) (PF8),[62,63] created through oxidation of a fluorene monomer, also acts as efficient electron trap.[64] However, these authors already observe a trap-dominated electron current for defect-free PF8. In contrast, the results of the previous section show that rather small changes of the molecular structure of either the side chains or the backbone of the PFTBTT copolymer investigated here causes the disappearance of the mobility relaxation, making it unlikely that the electron traps are originating from doping, chemical defects, or impurities. Thus, we suppose that in our case, the electron traps causing the mobility relaxation in alt-PF8TBTT must be related to the microscopic morphology or the molecular design of the copolymer itself. It was recently noted that solar cells of the high-performance donor material poly[N-9′-hepta-decanyl-2,7-carbazole-alt-5,5-(4′,7′-di-2-thienyl-2′,1′,3′-benzothiadiazole)] (PCDTBT) may suffer from significant intrinsic trapping of free charge carriers, introduced by morphological changes of the PCDTBT phase.[65,66] Here, we note the great chemical similarity of PCDTBT and alt-PF8TBTT, only differing by two atoms (the nitrogen or carbon atom at the bridge position of the carbazole or fluorene monomer, respectively, and an additional carbon atom that mediates the dioctyl substitution with the bridging nitrogen atom in PCDTBT). Through measurement of the paracrystalline disorder and in combination with density functional theory-based molecular simulations, a connection between the microscopic morphology and the development of exponentially distributed trap states was also recently proposed by Rivnay *et al.*[67]

An alternative explanation for the particular trapping properties of alt-PF8TBTT arises from work by Dieckmann *et al.* These authors showed that the electrostatic interactions of transport sites and randomly oriented dipoles can cause a significant broadening of the DOS.[68] Such permanent dipoles might be created via intermolecular coulombic interactions between the electron-attracting TBTT (acceptor) unit and the electron-withdrawing fluorene (donor) group of neighboring chains, driven by π–π stacking. A particularly favorable situation would occur if neighboring chains in a stack were shifted by half a repeat unit, a pattern that may be introduced due to the sp^3 hybridization of the side chain-containing bridging atom, which forces the side chains to stick out of the plane of the polymer backbone.[21] The regular donor/acceptor stacking and the proximity of neighboring chains might be altered by attaching longer side chains (as in alt-PF8/12TBTT) or by disturbing the regular alternation of donor and acceptor units along the backbone (as in part-PF8TBTT). In this context, other dioctyl-substituted fluorene copolymers show pronounced electron trapping. Namely, electron trapping is demonstrated for pure poly(9,9′-dioctylfluorene-co-benzothiadiazole),[47,54] F8TBT,[29,30] and finally, in this study, for alt-PF8TBTT. In contrast copolymers that perform best in devices carry longer or branched substituents.[19–21,23,69,70]

V. CONCLUSIONS

We performed various transient photocurrent experiments on a model donor/acceptor copolymer. Our measurements reveal time-dependent electron mobility. The origin of the strong mobility relaxation was identified by a multiple trapping model–based MC simulation and is explained by the significant trapping of electrons. It is further demonstrated that the electron trapping has a severe influence on the shape of the current transients. Chemical modifications of the polymers structure revealed the origin of the electron trapping to be related to the molecular structure, specific morphology, or both of the copolymer. Our results show that small changes of the molecular design of donor/acceptor copolymers can introduce electronic trap states with severe impact on their charge transport properties.

ACKNOWLEDGMENTS

The authors thank Sylvia Janietz (Frauenhofer Institute for Applied Polymer Research, Potsdam) for providing a batch of alt-PF8TBTT, and Heinz Bässler and Anna Köhler for directing our attention to the influence of dipolar interactions on charge transport. We also acknowledge laboratory assistance by Steffen Roland. M.S. and E.P. acknowledge funding by the German Research Foundation within Priority Program No. SPP 1355.

[1]H. Bässler, Phys. Status Solidi B **175**, 15 (1993).
[2]T. Tiedje and A. Rose, Solid State Comm. **37**, 49 (1981).
[3]P. W. M. Blom and M. Vissenberg, Mater. Sci. Eng. R Rep. **27**, 53 (2000).
[4]C. Tanase, E. J. Meijer, P. W. M. Blom, and D. M. de Leeuw, Phys. Rev. Lett. **91**, 216601 (2003).
[5]W. F. Pasveer, J. Cottaar, C. Tanase, R. Coehoorn, P. A. Bobbert, P. W. M. Blom, D. M. de Leeuw, and M. A. J. Michels, Phys. Rev. Lett. **94**, 206601 (2005).
[6]V. I. Arkhipov, P. Heremans, E. V. Emelianova, and H. Bässler, Phys. Rev. B **71**, 045214 (2005).
[7]R. Coehoorn, W. F. Pasveer, P. A. Bobbert, and M. A. J. Michels, Phys. Rev. B **72**, 155206 (2005).
[8]I. Lange, J. C. Blakesley, J. Frisch, A. Vollmer, N. Koch, and D. Neher, Phys. Rev. Lett. **106**, 216402 (2011).
[9]J. Hwang, E. G. Kim, J. Liu, J. L. Bredas, A. Duggal, and A. Kahn, J. Phys. Chem. C **111**, 1378 (2007).
[10]P. M. Borsenberger, L. Pautmeier, and H. Bässler, J. Chem. Phys. **94**, 5447 (1991).
[11]A. J. Mozer, G. Dennler, N. S. Sariciftci, M. Westerling, A. Pivrikas, R. Österbacka, and G. Juška, Phys. Rev. B **72**, 035217 (2005).
[12]R. U. A. Khan, D. Poplavskyy, T. Kreouzis, and D. D. C. Bradley, Phys. Rev. B **75**, 035215 (2007).
[13]J. Orenstein and M. Kastner, Phys. Rev. Lett. **46**, 1421 (1981).
[14]A. Devizis, A. Serbenta, K. Meerholz, D. Hertel, and V. Gulbinas, Phys. Rev. Lett. **103**, 027404 (2009).
[15]A. Devizis, K. Meerholz, D. Hertel, and V. Gulbinas, Phys. Rev. B **82**, 155204 (2010).
[16]A. Pivrikas, P. Stadler, H. Neugebauer, and N. S. Sariciftci, Org. Electron. **9**, 775 (2008).
[17]M. Schubert, R. Steyrleuthner, S. Bange, A. Sellinger, and D. Neher, Phys. Status Solidi A **206**, 2743 (2009).
[18]M. Svensson, F. L. Zhang, S. C. Veenstra, W. J. H. Verhees, J. C. Hummelen, J. M. Kroon, O. Inganäs, and M. R. Andersson, Adv. Mater. **15**, 988 (2003).
[19]L. H. Slooff, S. C. Veenstra, J. M. Kroon, D. J. D. Moet, J. Sweelssen, and M. M. Koetse, Appl. Phys. Lett. **90**, 143506 (2007).
[20]M. H. Chen, J. Hou, Z. Hong, G. Yang, S. Sista, L. M. Chen, and Y. Yang, Adv. Mater. **21**, 4238 (2009).
[21]J. Liu, H. Choi, J. Y. Kim, C. Bailey, M. Durstock, and L. Dai, Adv. Mater. **24**, 538 (2011).
[22]D. Veldman, S. C. J. Meskers, and R. A. J. Janssen, Adv. Funct. Mater. **19**, 1939 (2009).
[23]D. Mori, H. Benten, J. Kosaka, H. Ohkita, S. Ito, and K. Miyake, ACS Appl. Mater. Interfac. **3**, 2924 (2011).
[24]X. M. He, F. Gao, G. L. Tu, D. Hasko, S. Huttner, U. Steiner, N. C. Greenham, R. H. Friend, and W. T. S. Huck, Nano Lett. **10**, 1302 (2010).
[25]M. Koppe, H. J. Egelhaaf, G. Dennler, M. C. Scharber, C. J. Brabec, P. Schilinsky, and C. N. Hoth, Adv. Funct. Mater. **20**, 338 (2010).
[26]C. Muller, E. G. Wang, L. M. Andersson, K. Tvingstedt, Y. Zhou, M. R. Andersson, and O. Inganäs, Adv. Funct. Mater. **20**, 2124 (2010).
[27]D. J. D. Moet, M. Lenes, J. D. Kotlarski, S. C. Veenstra, J. Sweelssen, M. M. Koetse, B. de Boer, and P. W. M. Blom, Org. Electron. **10**, 1275 (2009).
[28]C. R. McNeill and N. C. Greenham, Appl. Phys. Lett. **93**, 203310 (2008).
[29]I. Hwang, C. R. McNeill, and N. C. Greenham, J. Appl. Phys. **106**, 094506 (2009).
[30]Z. Li, F. Gao, N. C. Greenham, and C. R. McNeill, Adv. Funct. Mater. **21**, 1419 (2011).
[31]J. A. Letizia, M. R. Salata, C. M. Tribout, A. Facchetti, M. A. Ratner, and T. J. Marks, J. Am. Chem. Soc. **130**, 9679 (2008).
[32]R. C. Mulherin, S. Jung, S. Huettner, K. Johnson, P. Kohn, M. Sommer, S. Allard, U. Scherf, and N. C. Greenham, Nano Lett. **11**, 4846 (2011).
[33]H.-G. Nothofer, Flüssigkristalline Polyfluorene, Dissertation, University of Potsdam, Potsdam, http://opus.kobv.de/ubp/volltexte/2005/24/ (2001).
[34]V. P. Baillargeon and J. K. Stille, J. Am. Chem. Soc. **108**, 452 (1986).
[35]J. H. Li, Y. Liang, D. P. Wang, W. J. Liu, Y. X. Xie, and D. L. Yin, J. Org. Chem. **70**, 2832 (2005).
[36]S. Ellinger, U. Ziener, U. Thewalt, K. Landfester, and M. Moller, Chem. Mat. **19**, 1070 (2007).
[37]L. L. Chua, J. Zaumseil, J. F. Chang, E. C. W. Ou, P. K. H. Ho, H. Sirringhaus, and R. H. Friend, Nature **434**, 194 (2005).
[38]C. Yin, B. Pieper, B. Stiller, T. Kietzke, and D. Neher, Appl. Phys. Lett. **90**, 133502 (2007).
[39]D. M. Huang, S. A. Mauger, S. Friedrich, S. J. George, D. Dumitriu-LaGrange, S. Yoon, and A. J. Moule, Adv. Funct. Mater. **21**, 1657 (2011).
[40]S. Bange, M. Schubert, and D. Neher, Phys. Rev. B **81**, 035209 (2010).
[41]N. Metropolis and S. Ulam, J. Am. Stat. Assoc. **44**, 335 (1949).
[42]A. Miller and E. Abrahams, Phys. Rev. **120**, 745 (1960).
[43]L. M. Andersson, F. L. Zhang, and O. Inganäs, Appl. Phys. Lett. **91**, 071108 (2007).
[44]C. R. McNeill, A. Abrusci, J. Zaumseil, R. Wilson, M. J. McKiernan, J. H. Burroughes, J. J. M. Halls, N. C. Greenham, and R. H. Friend, Appl. Phys. Lett. **90**, 193506 (2007).
[45]G. Juška, K. Arlauskas, M. Viliunas, K. Genevicius, R. Österbacka, and H. Stubb, Phys. Rev. B **62**, R16235 (2000).
[46]R. Österbacka, A. Pivrikas, G. Juška, K. Genevicius, K. Arlauskas, and H. Stubb, Curr. Appl. Phys. **4**, 534 (2004).
[47]G. C. Faria, R. M. Faria, E. R. deAzevedo, and H. von Seggern, J. Phys. Chem. C **115**, 25479 (2011).
[48]G. Juška, K. Arlauskas, M. Viliunas, and J. Kocka, Phys. Rev. Lett. **84**, 4946 (2000).

[49]C. Deibel, A. Wagenpfahl, and V. Dyakonov, Phys. Rev. B **80**, 075203 (2009).
[50]D. Hertel and H. Bässler, ChemPhysChem **9**, 666 (2008).
[51]J. Frisch, M. Schubert, E. Preis, J. P. Rabe, D. Neher, U. Scherf, and N. Koch, J. Mater. Chem. **22**, 4418 (2012).
[52]J. Kniepert, M. Schubert, J. C. Blakesley, and D. Neher, J. Phys. Chem. Lett. **2**, 700 (2011).
[53]A. Kumar, M. A. Baklar, K. Scott, T. Kreouzis, and N. Stingelin-Stutzmann, Adv. Mater. **21**, 4447 (2009).
[54]R. Steyrleuthner, S. Bange, and D. Neher, J. Appl. Phys. **105**, 064509 (2009).
[55]P. Mark and W. Helfrich, J. Appl. Phys. **33**, 205 (1962).
[56]Z. Zhu, D. Waller, R. Gaudiana, M. Morana, D. Muhlbacher, M. Scharber, and C. Brabec, Macromolecules **40**, 1981 (2007).
[57]W. C. Germs, J. J. M. van der Holst, S. L. M. van Mensfoort, P. A. Bobbert, and R. Coehoorn, Phys. Rev. B **84**, 165210 (2011).
[58]L. Pautmeier, R. Richert, and H. Bässler, Philos. Mag. Lett. **59**, 325 (1989).
[59]G. Juška, N. Nekrasas, V. Valentinavicius, P. Meredith, and A. Pivrikas, Phys. Rev. B **84**, 155202 (2011).
[60]J. Orenstein and M. A. Kastner, Solid State Comm. **40**, 85 (1981).
[61]H. T. Nicolai, M. Kuik, G. A. H. Wetzelaer, B. de Boer, C. Campbell, C. Risko, J. L. Brédas, and P. W. M. Blom, Nat. Mater. **11**, 882 (2012).
[62]U. Scherf and E. J. W. List, Adv. Mater. **14**, 477 (2002).
[63]E. Zojer, A. Pogantsch, E. Hennebicq, D. Beljonne, J. L. Bredas, P. S. de Freitas, U. Scherf, and E. J. W. List, J. Chem. Phys. **117**, 6794 (2002).
[64]M. Kuik, G. Wetzelaer, J. G. Ladde, H. T. Nicolai, J. Wildeman, J. Sweelssen, and P. W. M. Blom, Adv. Funct. Mater. **21**, 4502 (2011).
[65]Z. M. Beiley, E. T. Hoke, R. Noriega, J. Dacuna, G. F. Burkhard, J. A. Bartelt, A. Salleo, M. F. Toney, and M. D. McGehee, Adv. Energy Mater. **1**, 954 (2011).
[66]T. M. Clarke, J. Peet, A. Nattestad, N. Drolet, G. Dennler, C. Lungenschmied, M. Leclerc, and A. J. Mozer, Org. Electron. **13**, 2639 (2012).
[67]J. Rivnay, R. Noriega, J. E. Northrup, R. J. Kline, M. F. Toney, and A. Salleo, Phys. Rev. B **83**, 121306 (2011).
[68]A. Dieckmann, H. Bässler, and P. M. Borsenberger, J. Chem. Phys. **99**, 8136 (1993).
[69]D. Veldman, O. Ipek, S. C. J. Meskers, J. Sweelssen, M. M. Koetse, S. C. Veenstra, J. M. Kroon, S. S. van Bavel, J. Loos, and R. A. J. Janssen, J. Am. Chem. Soc. **130**, 7721 (2008).
[70]J. Gilot, M. M. Wienk, and R. A. J. Janssen, Adv. Mater. **22**, E67 (2010).
[71]See Supplemental Material at http://link.aps.org/supplemental/10.1103/PhysRevB.87.024203 for additional experimental data.